

Interface control of ferroelectricity in $\text{LaNiO}_3\text{-BaTiO}_3$ superlattices

Yin-Zhong Wu^{1,3,*}, Hai-Shuang Lu², Tian-Yi Cai² & Sheng Ju^{2,†}

¹*Jiangsu Laboratory of Advanced Functional Materials and Physics Department,
Changshu Institute of Technology, Changshu 215500, P. R. China,*

²*Department of Physics and Jiangsu Key Laboratory of Thin Films,
Soochow University, Suzhou 215006, P. R. China,*

³*School of Mathematics and Physics,
Suzhou University of Science and Technology, Suzhou 215009, P. R. China*

Abstract

$\text{LaNiO}_3\text{-BaTiO}_3$ superlattices with different types of interfaces are studied from first-principles density-functional theory. It is revealed that the ferroelectricity in the superlattice with $(\text{NiO}_2)^{-}/(\text{BaO})^0$ interfaces is enhanced from that of the superlattice with $(\text{LaO})^{+}/(\text{TiO}_2)^0$ interfaces. The origin lies at the polar discontinuity at the interface, which makes the holes localized within the $(\text{NiO}_2)^{-}/(\text{BaO})^0$ interface, but drives a penetration of electrons into BaTiO_3 component near $(\text{LaO})^{+}/(\text{TiO}_2)^0$ interface. Our calculations demonstrate an effective avenue to the robust ferroelectricity in BaTiO_3 ultrathin films.

PACS numbers: 77.80.bn, 77.55.fe, 77.55.Px, 73.20.-f

Keywords: LaNiO_3 , BaTiO_3 , carrier doping, ferroelectricity, and first-principles

* Electronic address: yzwu@cslg.edu.cn

† Electronic address: jusheng@suda.edu.cn

I. INTRODUCTION

Ferroelectric ultrathin films and heterostructure have attracted great interest in recent years¹⁻¹⁴. The ferroelectricity, in particular, the critical thickness, was found depend strongly on the proper choice of the interface. By controlling the chemical bonding at the interface, both the enhanced and decreased ferroelectricity have been found in BaTiO₃ and PbTiO₃ ultrathin films. In fact, polar discontinuity at the heterointerface widely exists at oxide based heterostructures¹⁵⁻²⁰. Generally, it will lead to carrier doping in formerly insulating component and consequently emergent electronic phase, e.g., conducting two-dimensional electron gas in LaAlO₃-SrTiO₃ heterointerface. For ferroelectric materials, as studied in the BaTiO₃ bulk system²¹, such a kind of carrier doping will strongly decrease the ferroelectricity, equally for the electron doping and the hole doping. In the heterostructures or ferroelectric ultrathin films, however, the situation is yet not clear. In all the previous studies of the ferroelectric ultrathin films¹⁻¹², metallic electrode either of SrRuO₃ (with alternating (SrO)⁰ and (RuO₂)⁰ layers) or Pt shows no polar features.

Generally, as demonstrated in Fig. 1, the charge and potential diagrams in the metal-ferroelectrics superlattice can be simply described by a screening model. The charge distribution of symmetric metal-ferroelectrics interfaces with normal metal, such as Pt and Au, is illustrated in Fig. 1(a) with corresponding potential energy in Fig. 1(d). However, if a positively charged layer (e.g. the (LaO)⁺ layer) is allowed at the interface, then, screening electrons will accumulate at adjacent ferroelectric layer (see Fig. 1(b), here spontaneous polarization is set zero for clarity), and an inhomogeneous electron doping will take place in the ferroelectric component. Taking the polarization into account, as illustrated in Fig. 1(e), the potential profile is the superposition of them. On the other hand, for a negatively charged layer, similarly asymmetric potential but with reversal sign is shown in Fig. 1(f). Such a picture suggests that the ferroelectric performance in the thin film geometry should be the same for electron doping case and hole doping one, the situation of which is similar to the bulk system²¹.

In order to check the validity of the above picture, we use LaNiO₃ as electrode with alternating charged layers of (LaO)⁺ and (NiO₂)⁻. Perovskite oxide LaNiO₃ is structurally compatible with ferroelectric BaTiO₃, and ferroelectric thin films with LaNiO₃ electrodes were found to possess better fatigue properties compared with other metallic oxides^{22,23}.

As shown in Fig. 2, LaNiO₃-BaTiO₃ superlattices are proposed. Here, two types of polar discontinuities are clearly distinguished, namely (LaO)⁺/(TiO₂)⁰ with positive charge and (NiO₂)⁻/(BaO)⁰ negative one, which correspond to the situation described in Fig. 1(b) and (c), respectively. In the following, we will provide a systematic first-principles study of atomic and electronic structures in these LaNiO₃-BaTiO₃ superlattices. Our calculations provide solid evidence of contrast between electron doping and hole doping in nanoscale ferroelectrics.

II. SYSTEMS AND METHODS

Our *ab initio* calculations are performed using the full-potential projector-augmented wave (PAW) method²⁴, as implemented in the Vienna *ab initio* simulation package (VASP)²⁵. They are based on local density-approximation, which can describe both ferroelectric BaTiO₃ and electrode LaNiO₃ well²⁶. A plane-wave cutoff of 500 eV is used throughout, and atomic relaxations are converged using 10 × 10 × 1 Monkhorst-Pack k-point sampling of Brillouin zone until the maximum Hellman-Feynman force acting on each atom is less than 0.01 eV/Å. PAW potentials are used to describe the electron-ion interaction with 9 valence electrons for La (5p⁶5d¹6s²), 16 for Ni (3p⁶3d⁸4s²), 10 for Ba (5s²5p⁶6s²), Ti (3p⁶3d²4s²), and 6 for O (2s²2p⁴). Superlattice is (001) epitaxially grown on SrTiO₃ substrate with the in-plane lattice constant of 3.866 Å. The superlattice structures we use are [LaO-(NiO₂-LaO)₁₀/(TiO₂-BaO)_m-TiO₂] and [NiO₂-(LaO-NiO₂)₁₀/(BaO-TiO₂)_m-BaO], as shown in Fig. 2 for $m = 3$. The (LaO)⁺/(TiO₂)⁰ interface here is similar to (LaO)⁺/(TiO₂)⁰ in LaAlO₃-SrTiO₃ superlattice¹⁸ and (NbO₂)⁺/(SrO)⁰ interface in KNbO₃-SrTiO₃ superlattice¹⁹. And the second type interface (NiO₂)⁻/(BaO)⁰ has not been reported in the literature.

III. RESULTS AND DISCUSSIONS

First, we study the inherent ferroelectric displacement and its evolution with the thickness of ferroelectric layer. In Fig. 3(a)-(f) and 3(g)-(l), the relative cation-anion displacements within both LaNiO₃ and BaTiO₃ are plotted. In BaTiO₃, the spontaneous polarization is proportional to the relative cation-anion displacements³. Here, the existence of ferroelec-

tricity in ferroelectric barrier is determined by the non-zero total polarization of the whole BaTiO₃ barrier¹¹. Clearly, for (LaO)⁺/(TiO₂)⁰ interfaces, one can see that the BaTiO₃ film is paraelectric (PE) when the thickness of BaTiO₃ is smaller than six unit cells. On the other hand, for the case of (NiO₂)⁻/(BaO)⁰ interfaces, the ferroelectricity of BaTiO₃ film will be preserved down to the thickness of four unit cells. The above results differ greatly from the SrRuO₃-BaTiO₃-SrRuO₃ capacitor, where the critical thickness of BaTiO₃ film with SrO/TiO₂ interfaces is thinner than that of BaTiO₃ film with RuO₂/BaO interfaces⁹. The polarity-discontinuity at metal-ferroelectric interfaces is therefore dominating. In addition, the relative cation-anion displacements for $m = 8$ approach the bulk value of BaTiO₃.

To gain a deeper insight into the above differences, electronic structure of local density of state is plotted in Fig. 4 for the superlattice (LaNiO₃)_{10.5}-(BaTiO₃)_{3.5}, where the BaTiO₃ film stays on paraelectric(PE) state as illustrated in Fig. 3, Thus, the effect of polar discontinuity on the DOS of BaTiO₃ is investigated without consideration of the influence of spontaneous polarization at the first step. The layer-projected DOS are centrosymmetric for both two types of interfaces. For (LaO)⁺/(TiO₂)⁰ interfaces in Fig. 4(a), the Fermi energy is pushed into the bottom of conduction band, which is similar to the positively charged (LaO)⁺ doped in SrRuO₃-BaTiO₃-SrRuO₃ junctions⁶. Due to the discontinuity of polarity, electrons transfer from the metal to BaTiO₃ film to neutralize the polarity, and charge leakage will suppress polarization of FE film by producing a ferroelectrically dead layer. Here, the doping is inhomogeneous among the interface and the interior of BaTiO₃ film. Things will be different for (NiO₂)⁻/(BaO)⁰ polarity-discontinuity interfaces in Fig. 4(b), where Fermi energy shifts to the top of valence band of BaTiO₃, and the interfacial BaO layer becomes obviously metallic, which is induced by the hole doping in the interfacial BaO layer. If the DOS of the interfacial BaTiO₃ layer is conductive, then we say the interface is metallic, i.e., the contact between the electrode and BaTiO₃ barrier is Ohmic contact¹³. Similarly, when the DOS of the interfacial BaTiO₃ layer is insulative, then a tunneling barrier is formed at the interface, which has also been defined in Ref. 13 for SrRuO₃/ n -BaTiO₃ interface.

With the presence of polarization in Fig. 5 for the superlattice (LaNiO₃)_{10.5}-(BaTiO₃)_{8.5} with the ferroelectric polarization pointing to the right, an asymmetric distribution of electronic states is found, with the valence band near the left interface upward and the conduction band near the right interface downward. For the superlattice with (LaO)⁺/(TiO₂)⁰

interfaces in Fig. 5(a), ferroelectric polarization controls the accumulation or depletion of electrons near the left and right interfaces, and it is found that the right interface is ohmic contact, while the left interface turns to Schottky tunnel barrier with the development of ferroelectricity in the BaTiO₃ component. The left and right interfaces are both ohmic contact for PE state as shown in Fig. 4(a). For the case of (NiO₂)⁻/(TiO₂)⁰ interfaces in Fig. 5(b), the left interface and right interface are always keeping as ohmic contact regardless of the appearance of spontaneous polarization.

The number of accumulated charges, either the electrons of occupied Ti *d* orbital in TiO₂ layer or O *p* orbital in BaO layer for (LaNiO₃)_{10.5}-(BaTiO₃)_{8.5} superlattice, is integrated and shown in Fig. 6. For the superlattice with (LaO)⁺/(TiO₂)⁰ interfaces, the polar layer of (LaO)⁺ leads to a four electron-doped BaTiO₃ layers at the right ($d_e = 4$). For the superlattice with (NiO₂)⁻/(TiO₂)⁰ interface, on the other hand, the holes are restricted at one unit cell ($d_{hL} = d_{hR} = 1$) and the magnitude at both sides is much larger than the electron doped cases. Obviously, for the strong itinerant nature of (NiO₂)⁻ layer, the holes are absorbed in Fermi sea of the LaNiO₃ electrodes. These findings are different from SrTiO₃-LaAlO₃ heterointerface, where the holes delocalize into SrTiO₃ at p-type interface and electrons in n-type interface¹⁷.

In fact, the value d_e and d_h are found independent of the thickness of BaTiO₃, i.e., the occurrence of polarization in BaTiO₃ has little influence on the depth of hole-doping. With the above analysis, the contrast between electron doping and hole doping is evident in nanoscale ferroelectrics. The electrostatic potential as demonstrated in Fig. 1(c) is therefore improper for the LaNiO₃-BaTiO₃ superlattice with (NiO₂)⁻/(BaO)⁰ interfaces, where a more symmetric situation is expected. The polar discontinuity can be neutralized via interface electronic reconstruction at oxide heterointerface, however, for the metal-ferroelectric heterostructure only electrons can penetrate into BaTiO₃ component. Such differences also lead to variation of ferroelectric critical thickness, which is 4 for hole-doped case and 6 for electron-doped case.

In summary, ferroelectricity in LaNiO₃-BaTiO₃ superlattices with polar discontinuity at the interfaces are investigated from first-principles. It is found that the polar discontinuity in the (NiO₂)⁻/(TiO₂)⁰ interface is neutralized within the interface, in contrast to the case of (LaO)⁺/(TiO₂)⁰ interface, where the screening electron can penetrate into the

BaTiO₃ layer of four unit cells. Such differences make the ferroelectricity in the ultrathin films with (NiO₂)⁻/(BaO)⁰ interface much stronger than that in the ultrathin films with (LaO)⁺/(TiO₂)⁰ interfaces, therefore, providing an avenue to realize the interface control of ferroelectricity as well as functionalities in ferroelectric nanodevices.

Acknowledgments Y. Z. Wu thanks Prof. Valeriy Stepanyuk for discussions during visiting Max Planck Institute of Microstructure Physics. S. Ju appreciates Dr. Gaoyang Gou for the helpful discussion on LaNiO₃. This work was supported by the National Science Foundation of China (Grant Nos. 11274054, 11374220, 11104193, and 11174043), and the 333 project of Jiangsu Province.

-
- ¹J. Junquera and P. Ghosez, *Nature (London)* **422**, 506 (2003).
- ²N. Sai, A. M. Kolpak, and A. M. Rappe, *Phys. Rev. B* **72**, 020101(R) (2005).
- ³G. Gerra, A. K. Tagantsev, N. Setter, and K. Parlinski, *Phys. Rev. Lett.* **96**, 107603 (2006).
- ⁴C. G. Duan, R. F. Sabirianov, W. N. Mei, S. S. Jaswal, and E. Y. Tsymbal, *Nano Lett.* **6**, 483 (2006).
- ⁵M. Stengel, D. Vanderbilt, and N. A. Spaldin, *Nature Mater.* **8**, 392 (2009).
- ⁶Y. Wang, M. K. Niranjana, K. Janicka, J. P. Velev, S. S. Jaswal, and E. Y. Tsymbal, *Phys. Rev. B* **82**, 094114 (2010).
- ⁷W. A. Al-Saidi, and A. M. Rappe, *Phys. Rev. B* **82**, 155304 (2010).
- ⁸M. Stengel, P. Aguado-Puente, N. A. Spaldin, and J. Junquera, *Phys. Rev. B* **83**, 235112 (2011).
- ⁹X. Liu, Y. Wang, P. V. Lukashev, J. D. Burton, and E. Y. Tsymbal, *Phys. Rev. B* **85**, 125407 (2012).
- ¹⁰X. Liu, Y. Wang, J. D. Burton, and E. Y. Tsymbal, *Phys. Rev. B* **88**, 165139 (2013).
- ¹¹W. J. Chen, Y. Zheng, X. Luo, B. Wang, and C. H. Woo, *J. Appl. Phys.* **114**, 064105 (2013).
- ¹²L. Shen, T. J. Zhou, Z. Q. Bai, M. G. Zeng, J. Q. Goh, Z. M. Yuan, G. H. Han, B. Liu, and Y. P. Feng, *Phys. Rev. B* **85**, 064105 (2012).
- ¹³V. R. Cooper, K. Johnston, and K. M. Rabe, *Phys. Rev. B* **76**, 020103(R) (2007).
- ¹⁴X. F. Wu, K. M. Rabe, and D. Vanderbilt, *Phys. Rev. B* **83**, 020104(R) (2011).
- ¹⁵J. Heber, *Nature* **459**, 28 (2009).
- ¹⁶H. Chen, and S. Ismail-Beigi, *Adv. Mater.* **22**, 2881 (2010).
- ¹⁷H. Chen, A. M. Kolpak, and S. Ismail-Beigi, *Phys. Rev. B* **79**, 161402(R) (2009).
- ¹⁸K. Janicka, J. P. Velev, and E. Y. Tsymbal, *Phys. Rev. Lett.* **102**, 106803 (2009).
- ¹⁹M. K. Niranjana, Y. Wang, S. S. Jaswal, and E. Y. Tsymbal, *Phys. Rev. Lett.* **103**, 016804 (2009).
- ²⁰F. Hou, T. Y. Cai, S. Ju, and M. R. Shen, *ACS Nano* **6**, 8552 (2012).
- ²¹Y. Wang, X. Liu, J. D. Burton, S. S. Jaswal, and E. Y. Tsymbal, *Phys. Rev. Lett.* **109**, 247601 (2012).
- ²²J. J. Zhu, W. W. Li, Y. W. Li, Y. D. Shen, Z. G. Hu, and J. H. Chu, *Appl. Phys. Lett.* **97**,

211904 (2010).

²³H. Han, J. Zhong, S. Kotru, P. Padmini, X. Y. Song, and R. K. Pandey, *Appl. Phys. Lett.* **88**, 092902 (2006).

²⁴P. E. Blöchl, *Phys. Rev. B* **50** 17953 (1994).

²⁵G. Kresse and J. Furthmüller, *Comput. Mater. Sci.* **6**, 15 (1996).

²⁶G. Gou, I. Grinberg, A. M. Rappe, and J. M. Rondinelli, *Phys. Rev. B* **84**, 144101 (2011).

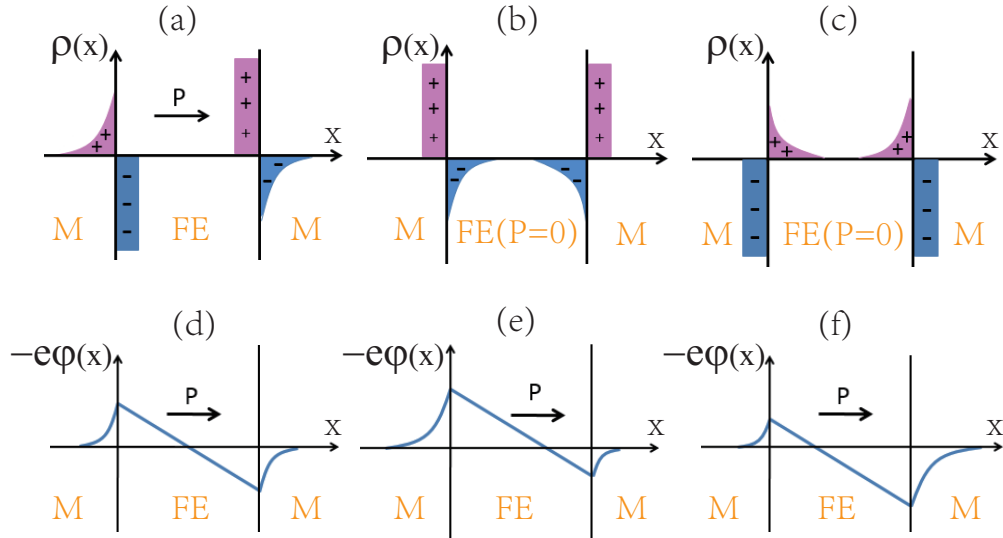


FIG. 1: Illustration of charge distribution and potential energy profile for metal-ferroelectric heterostructures. (a) Electrode of normal metal. Oxide electrode with polar discontinuity at the interface with (b) positively charged layer and (c) negatively charged layer. The potential energy profiles with the inclusion of spontaneous polarization are shown in (d), (e), and (f), respectively. In order to show the polar discontinuity and charge distribution clearly, the barrier polarization are not considered in (b) and (c), while the spontaneous polarization are included for the potential energy diagrams in (d), (e), and (f).

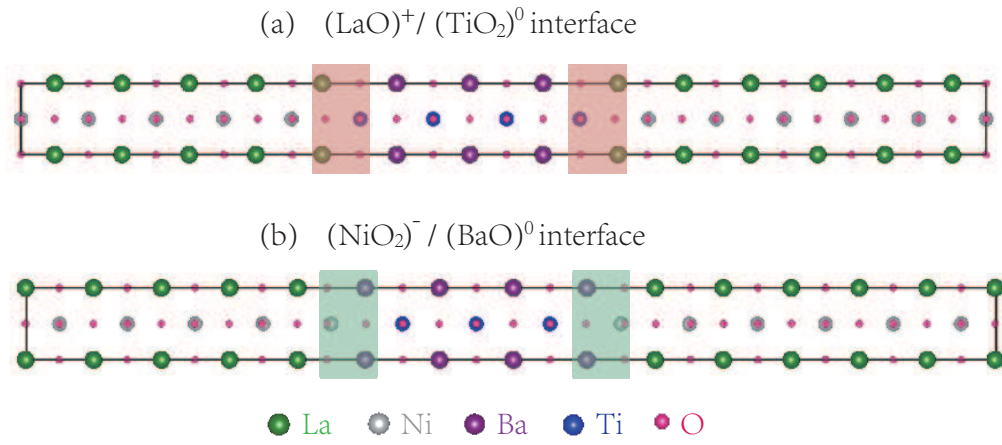


FIG. 2: Illustration of $\text{LaNiO}_3\text{-BaTiO}_3$ superlattice structure with (a) $(\text{LaO})^+ / (\text{TiO}_2)^0$ interface, and (b) $(\text{NiO}_2)^- / (\text{BaO})^0$ interface. Here, the thickness of BaTiO_3 is 3.5 unit cells.

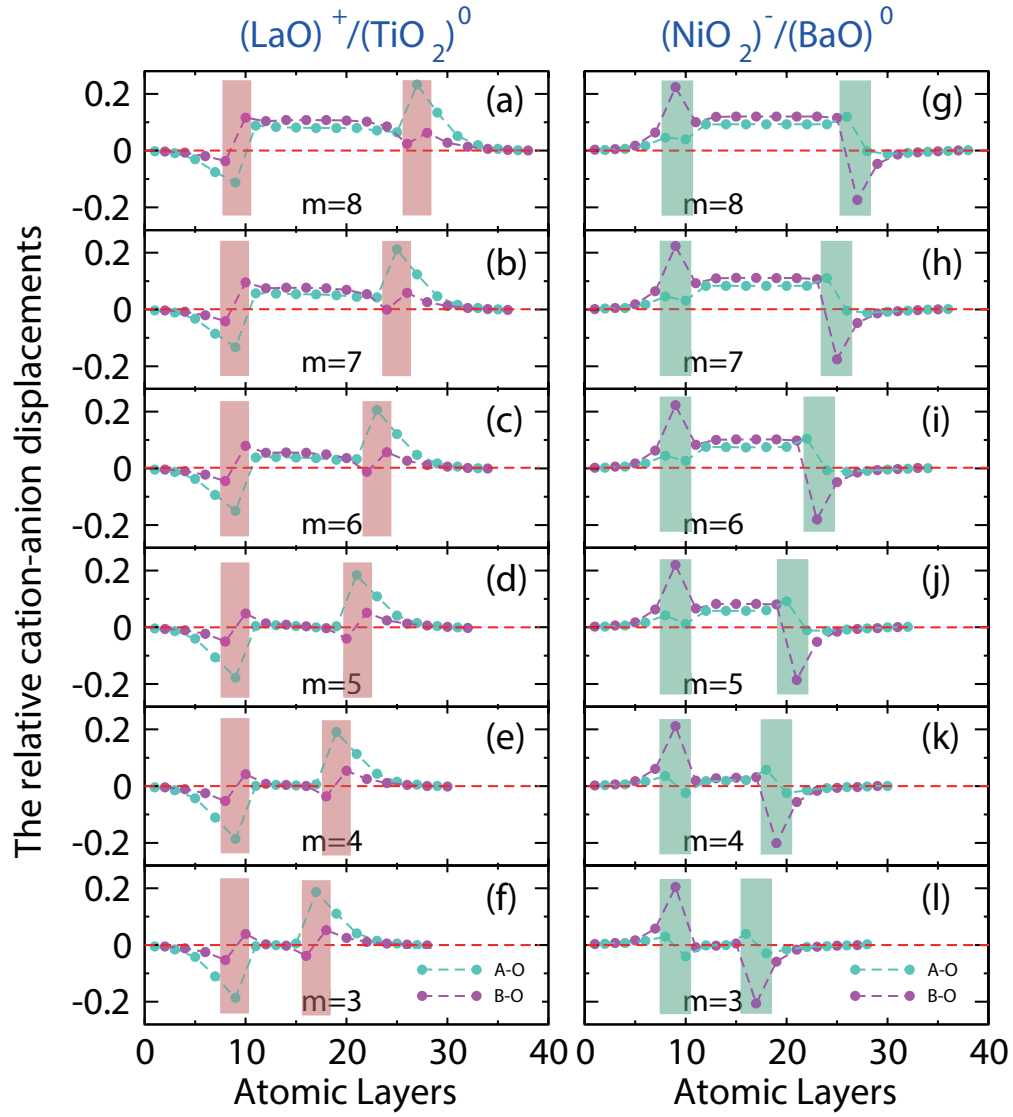


FIG. 3: [(a)-(f)] Relative A-O and B-O displacements in the optimized $[\text{LaO}-(\text{NiO}_2\text{-LaO})_{10}/(\text{TiO}_2\text{-BaO})_m\text{-TiO}_2]$ ($m = 8, 7, 6, 5, 4, 3$) superlattices. [(g)-(l)] $[\text{NiO}_2\text{-(LaO-NiO}_2)_{10}/(\text{BaO-TiO}_2)_m\text{-BaO}]$ ($m = 8, 7, 6, 5, 4, 3$) superlattices. Shadow regions represent the interfaces.

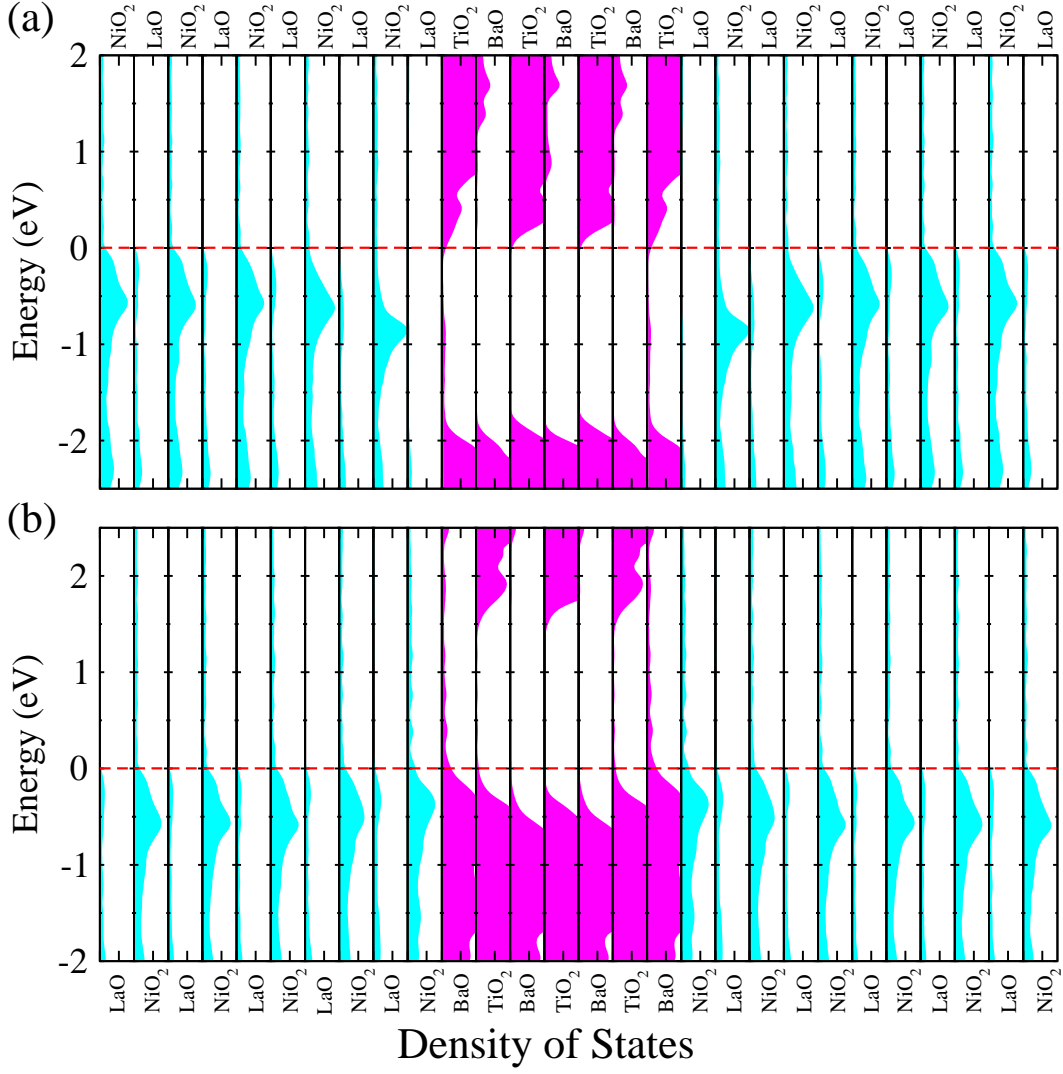


FIG. 4: Layer-projected density of states in $\text{LaNiO}_3\text{-BaTiO}_3$ superlattices ($m=3$) with (a) $(\text{LaO})^+ / (\text{TiO}_2)^0$ interfaces and (b) $(\text{NiO}_2)^- / (\text{BaO})^0$ interfaces. The scale of density of states in LaNiO_3 is nine times of that in BaTiO_3 . Here, the component BaTiO_3 stays on paraelectric state.

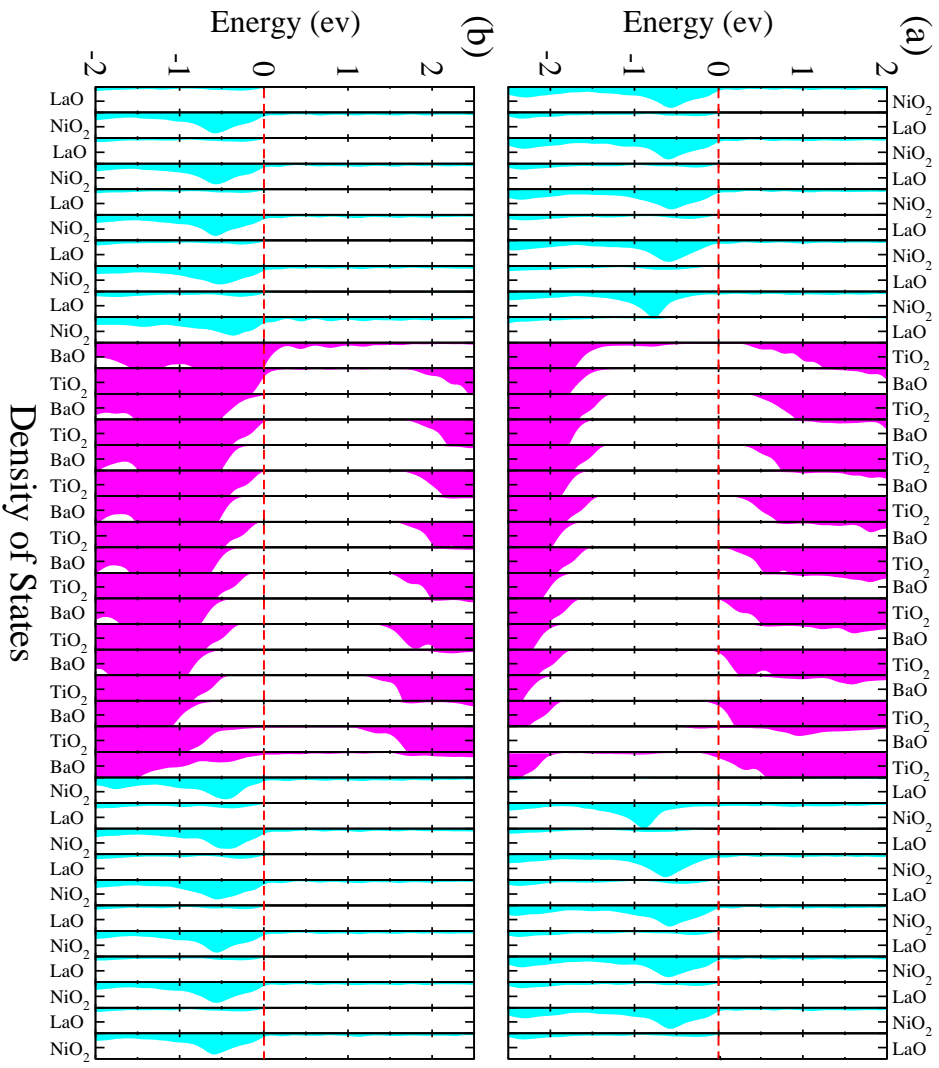


FIG. 5: Layer-projected density of states in $\text{LaNiO}_3\text{-BaTiO}_3$ superlattices ($m=8$) with (a) $(\text{LaO})^+ / (\text{TiO}_2)^0$ interfaces and (b) $(\text{NiO}_2)^- / (\text{BaO})^0$ interfaces. The scale of density of states in LaNiO_3 is nine times of that in BaTiO_3 .

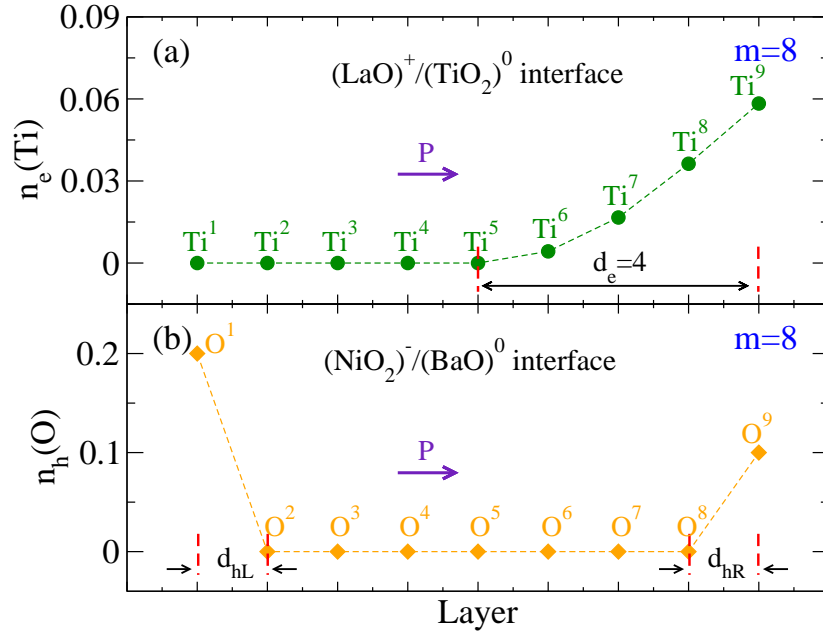


FIG. 6: (a) Number of electrons n_e integrated over Ti d orbital in conduction band of each TiO₂ monolayer. (b) Number of holes n_h integrated over O p orbital in the valence band of each BaO monolayer. Here, the thickness of BaTiO₃ component is 8.5 unit cells, and the polarization points to the right.